Paper:

Cheng, F and Dupont, V (2013) *Nickel catalyst auto-reduction during steam reforming of bio-oil model compound acetic acid.* International Journal of Hydrogen Energy, 38 (35). 15160 - 15172.

http://dx.doi.org/10.1016/j.ijhydene.2013.09.111

Nickel catalyst auto-reduction during steam reforming of bio-oil model compound acetic acid

Feng Cheng[*], Valerie Dupont

Energy Research Institute, School of Process, Environmental and Materials Engineering, The University of Leeds, Leeds LS2 9JT, UK

Abstract

Transition metal catalysts widely used in refineries are provided as oxides and require pre-reduction to become activated. The auto-reduction of a NiO/Al_2O_3 catalyst with acetic acid (HAc) followed by HAc steam reforming was investigated in a packed bed reactor. Effects of temperature and molar steam to carbon ratio (S/C) on reduction kinetics and catalyst performance were analysed. Results showed that a steady steam reforming regime along with complete NiO reduction could be obtained after a coexistence stage of reduction and reforming. A 2D nucleation and nuclei growth model fitted the NiO auto-reduction. The maximum reduction rate constant was attained at S/C=2. Steam reforming activity of the auto-reduced catalyst was just below that of the H_2-reduced catalyst, probably attributed to denser carbon filament formation and larger loss of active Ni. Despite this, a H_2 yield of 76.4% of the equilibrium value and HAc conversion of 88.97% were achieved at 750 °C and S/C=3.

Keywords

Nickel catalyst; auto-reduction; acetic acid; steam reforming; hydrogen production; carbon.

1. Introduction

Hydrogen production has attracted global attention because of hydrogen's growing application in proton exchange membrane fuel cells. At present, hydrogen generation processes including catalytic steam reforming of natural gas or naphtha, partial oxidation of heavy oil and steam gasification of coal have been well established. However, the reduction of fossil fuel stocks and the release of greenhouse gases caused by these processes have spurred research into sustainable and environmentally friendly hydrogen production routes. One promising route is to produce hydrogen from terrestrial biomass via fast pyrolysis followed by catalytic steam reforming of bio-oil or its fractions [1, 2]. Depending on biomass feedstock and pyrolysis conditions employed, the composition of bio-oil is varied but mainly consists of oxygenated hydrocarbons, such as acids, ketones, alcohols, phenols and sugars [2, 3]. In order to get a better understanding of the chemical process during steam reforming of the whole bio-oil, a number of studies have focused on steam

---

[*] Corresponding author. Tel.: +44 113 3432503; fax: +44 113 2467310.

  E-mail address: pmfc@leeds.ac.uk , V.Dupont@leeds.ac.uk

reforming of bio-oil model compounds [4-8], especially acetic acid (HAc) [9-14] due to its high content in bio-oil.

The steam reforming reaction is normally catalysed by supported transition metal catalysts (such as Co or Ni) or noble metal catalysts (Pt, Rh). For HAc steam reforming, a Ni based catalyst was found to have better stability and activity than other transition metal catalysts [11] and exhibited catalytic activity similar to that of noble metal catalysts [12]. To prevent potentially hazardous exothermic oxidation during transport or storage, transition metal catalysts are provided by manufacturers in the form of oxides instead of their active metallic state. Hence, they require to be reduced just prior to being used in steam reforming. In industry, this is achieved by subjecting the catalyst to a gaseous flow of H_2, NH_3, or CH_4, depending on their local availability [15]. In the latter case, a careful protocol of starting conditions with large excess of steam is recommended to avoid carbon deposits from CH_4 decomposition, which cause loss of active surface area [16]. Such a catalyst activation step does not only represent a starting regime which potentially relies on fossil feedstock (since both H_2 and NH_3 are at present produced at commercial scale mainly from natural gas) but also increase operational complexity, with its associated safety hazards. The present work intends to integrate catalyst reduction and steam reforming in one process (termed 'integrated process'). In this process, the oxidised catalyst is initially automatically reduced by reforming fuel in a period termed 'auto-reduction', and then sustains the steam reforming reaction. In particular, whether HAc, as a bio-oil model compound, has the ability to perform the reduction step will be investigated. To the authors' knowledge, little research has been done on the reduction of metal oxides by oxygenated hydrocarbons, although reduction with simple molecules such as H_2 [17-19], CH_4 [20-22] and CO [23] have been studied in the fields of metallurgy, catalysis and chemical looping technology.

Chemical looping reforming (CLR) is an advanced auto-thermal reforming technology for hydrogen production, which couples endothermic steam reforming and exothermic partial oxidation of reforming fuel by alternating fuel feed and oxidant feed (usually air) [16, 22, 24]. A well-designed CLR process could produce a non N_2-diluted syngas with low heating demand. During CLR, a supported metal oxide is used to perform two functions: (1) oxygen transfer via redox cycling and (2) catalysing steam reforming in its reduced state. Whether the reforming fuel employed is able to cyclically reduce the metal oxide at the beginning of fuel feed to initiate catalytic steam reforming is critical. Previous studies in this area mainly focused on screening suitable metal oxides based on their reduction reactivity with CH_4 [22, 25]. The reducing properties and mechanism of oxygenated hydrocarbons on metal oxide are less investigated, but quite significant for the potential application of renewable bio-feedstock in the CLR process.

In this paper, the feasibility of a NiO/Al_2O_3 catalyst auto-reduction by reforming feedstock HAc in an integrated process is examined using a packed bed reactor. The influence of reaction temperature and molar steam to carbon ratio (S/C) on the reduction kinetics as well as the subsequent steam reforming performance of HAc is also investigated. Moreover, the difference between the integrated process and conventional steam reforming process initiated by H_2 reduction is shown and

interpreted with focus on reforming activity, active Ni loss, carbon element distribution, and morphology of carbon deposits.

2. Experimental
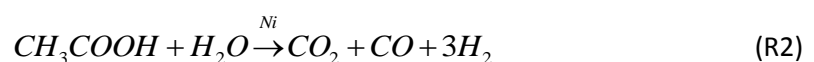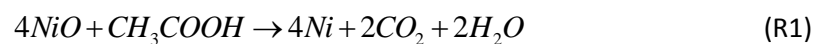
2.1 Materials and reactor set-up

The catalyst used in this study was 18 wt% NiO on α-Al$_2$O$_3$ (NiO/Al$_2$O$_3$) provided by Johnson Matthey Plc. The catalyst was received in pellet form and was broken and sieved to particle size range of 1.0-1.4 mm prior to use. Pure α-Al$_2$O$_3$ pellets were also provided by Johnson Matthey Plc and crushed into the same particle size so as to perform a control experiment. HAc with a purity of ≥99% was purchased from Sigma-Aldrich.
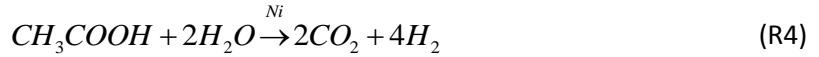
Steam reforming experiments were conducted in a down-flow packed bed reactor as shown in Fig. 1. For each run of experiment, 2 g fresh catalyst was placed in the middle of a quartz reactor, which was held inside a tube furnace. HAc aqueous solution with a given S/C ratio was injected into the reactor at a certain flow rate by a programmable syringe pump (New Era Pump Systems). The flow rate of gases (N$_2$ or H$_2$) was controlled by MKS mass flow rate controllers. The effluent was cooled via two condensers at -7 °C. Condensable gas products and unreacted water were trapped in a condensate collector, with moisture later removed by silica gel. After that, the composition of the dry reformate was recorded online at 5 second intervals using Advanced Optima analysers by ABB. These were capable of detecting H$_2$ by thermal conductivity (Caldos 15), and the carbon products CH$_4$, CO$_2$ and CO by infra-red absorption (Uras 14). A micro gas chromatograph (GC, equipped with MS5 and PPQ columns purchased from Agilent) was used to detect other possible hydrocarbon gases C$_2$ (C$_2$H$_4$, C$_2$H$_6$) and C$_3$ (C$_3$H$_6$, C$_3$H$_8$).

2.2 Experimental procedure

2.2.1 Integrated catalyst reduction and steam reforming process

This process was carried out at atmospheric pressure under a continuous N$_2$ flow of 200 sccm (as carrier gas) and in the absence of air. The reactor was heated to a set temperature, and HAc solution was fed into the reactor at a certain flow rate. Each experiment proceeded for about 45 min. The flow rate of liquid HAc was kept at 0.0336 ml/min for all runs of experiments. Different S/C ratios were achieved by changing water content in the HAc solution. NiO reduction by HAc (R1), HAc steam reforming reaction (R2) according to the mechanism proposed by Wang et al. [8] and water gas shift reaction (R3) are represented as follows. The overall stoichiometric reaction (R4) of steam reforming and water gas shift is also given.

$$4NiO + CH_3COOH \rightarrow 4Ni + 2CO_2 + 2H_2O \qquad \text{(R1)}$$

$$CH_3COOH + H_2O \overset{Ni}{\rightarrow} CO_2 + CO + 3H_2 \qquad \text{(R2)}$$

$$H_2O + CO \rightleftharpoons CO_2 + H_2 \qquad (R3)$$

$$CH_3COOH + 2H_2O \xrightarrow{Ni} 2CO_2 + 4H_2 \qquad (R4)$$

Reactions R1 to R4 merely show the global mechanisms of production of the main species CO, CO_2 and H_2 and reduced Ni but do not represent the actual, more complex mechanism involving adsorption of reactants, dissociation and formation of intermediates on the catalyst surface, recombination reactions, and desorption of products from the catalyst. In particular, reaction R2 is chosen here with co-production of CO_2 and CO as opposed to the more logical decomposition of HAc into 2CO and $2H_2$, to underline the observed early formation of CO_2 from HAc during steam reforming as discussed by Wang et al [8]. Once CO and H_2 appear in the products, they act in turn as reductants of NiO, but CO can also potentially methanate and disproportionate depending on prevalent local conditions. These result in formation of undesirable by-products CH_4 and solid carbon, which have slower kinetics of reaction with steam in the production of hydrogen.

2.2.2 Conventional steam reforming process (using H_2 to reduce catalyst)

After the reactor was heated to a certain temperature, the fresh catalyst was reduced by 5 %H_2/N_2 (R5). The completion of reduction was evidenced by H_2 concentration returning to 5%. After that, steam reforming of HAc was carried out as described in 2.2.1.

$$NiO + H_2 \rightarrow Ni + H_2O \qquad (R5)$$
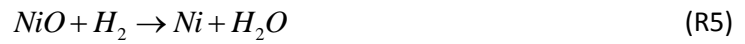
2.2.3 Elemental balance and definition of process outputs

Feedstock conversions, H_2 yield and reduction rate of NiO could be calculated on the basis of elemental balances. Equations and related assumptions for these calculations were described in [26] for fuel with a generic formula of $C_nH_mO_k$.

The molar flow rate of total dry outlet gas ($n_{out,dry}$) is estimated based on nitrogen balance (Eq. 1).

$$n_{out,dry} = \frac{n_{N_2}}{1 - y_{CH_4} - y_{CO} - y_{CO_2} - y_{H_2} - y_{C_2} - y_{C_3}} \qquad (Eq.\ 1)$$

HAc conversion (X_{HAc}) is calculated based on a carbon balance, by dividing the total molar flow of carbon in the gaseous products by the molar flow of carbon in feed, as described in Eq. 2.

$$X_{HAc}\ (\%) = 100 \times \frac{n_{out,dry} \times (y_{CO} + y_{CO_2} + y_{CH_4} + 2y_{C_2} + 3y_{C_3})}{2n_{HAc,in}} \qquad (Eq.\ 2)$$

H_2O conversion (X_{H2O}) is calculated based on a hydrogen balance (Eq. 3).

$$X_{H_2O}\left(\%\right) = 100 \times \frac{n_{out,dry} \times \left(2y_{CH_4} + y_{H_2} + 2y_{C_2H_4} + 3y_{C_2H_6} + 3y_{C_3H_6} + 4y_{C_3H_8}\right) - 2 \times n_{HAc,in} \times X_{HAc}}{n_{H_2O,in}} \qquad (Eq.\ 3)$$

H_2 yield is defined as the percentage of H_2 produced experimentally with respect to the theoretical maximum according to R4 (Eq. 4).

$$H_2 \, yield(\%) = 100 \times \frac{n_{out,dry} \times y_{H_2}}{4 n_{HAc,in}} \qquad \text{(Eq. 4)}$$

On the basis of an oxygen balance, Eq. 5 is used to evaluate the rate of NiO reduction to Ni.

$$reduction\,rate = n_{out,dry} \times \left(y_{CO} + 2 y_{CO_2} \right) - n_{H_2O,in} \times X_{H_2O} - 2 \times n_{HAc,in} \times X_{HAc} \qquad \text{(Eq. 5)}$$

The above rate equation (unit: mol/s) is integrated at a time interval of 5 seconds, yielding total moles of NiO reduced to Ni over a given duration. The extent of NiO conversion to Ni is then shown as a fraction of initial moles of Ni present in catalyst.

Nomenclature

n_i: molar flow rate of specie i
y_i: molar fraction of specie i in the dry outlet gas
X_i: conversion fraction of specie i
$$y_{C_2} = y_{C_2H_4} + y_{C_2H_6}, \qquad y_{C_3} = y_{C_3H_6} + y_{C_3H_8}$$

2.3 Characterization methods

X-ray diffraction (XRD) patterns of unreacted and reacted catalysts were obtained on PANalytical X'pert MPD instrument using Cu Kα radiation. Phase analysis based on the XRD data was conducted using the X'Pert HighScore Plus software. To quantify catalyst composition (respective amounts of Ni, NiO and Al_2O_3 present) as well as crystallites size, the Rietveld refinement method [27] was employed to analyse XRD data. The surface morphology of the reacted catalyst was investigated using a field-emission scanning electron microscope (FESEM, LEO Gemini 1530). Temperature-programmed oxidation (TPO) of the reacted catalyst was conducted on thermogravimetric analyser (TGA, TGH1000 by Stanton Redcroft). Meanwhile, CO_2 evolution due to carbon combustion in the TGA reactor was monitored using a Fourier transform infrared spectrometer (FTIR, Nicolet iS10 by Thermo Scientific). The TGA and FTIR instruments were integrated via a Nicolet manufactured transfer line. FTIR spectral scanning from 4000-500 cm^{-1} on gaseous products was repeated each 30 seconds as samples were heated at 10 °C/min from ambient temperature to 900 °C under air flow. The amount of carbon deposited on the reacted catalyst was measured by CHN Elemental Analyser (Flash EA2000 by CE Instruments). The catalyst needed to be crushed into fine powder for XRD, TGA-FTIR and CHN tests whereas catalyst particles coated with a platinum layer of 10 nm were used directly for FESEM imaging.

In addition to the aforementioned catalyst characterisation, the condensate liquid collected was also analysed. Total organic carbon (TOC) content in the condensate was measured using a Hach-Lange

IL550 analyser. Ni ion concentration in condensate was detected using an inductively coupled plasma mass spectrometry instrument (ICP-MS, SCIEX Elan 900 by Perkin Elmer).

2.4 Thermodynamic equilibrium calculations for steam reforming of HAc

Thermodynamic equilibrium calculations were performed based on minimisation of Gibbs free energy [28]. The thermodynamic properties of HAc were found in [29] while those of the other species (H_2O, CH_4, CO_2, CO, H_2, NH_3, NH_2, C_2H_6, C_2H_5, C_2H_4, C_2H_2, C_3H_8, C_3H_6, N_2, Ar) were from [30]. The gas equilibrium of HAc with water was calculated at atmospheric pressure from 0-750 °C at different S/C ratios to illustrate the effect of temperature or S/C ratio on steam reforming performance. A negligible molar fraction of Ar of 0.01 was included in the initial mixture to facilitate yields calculations.

3. Results and discussion

3.1 Auto-reduction of NiO by HAc

3.1.1 Process analysis

An integrated catalyst reduction and steam reforming experiment at 650 °C with S/C=3 was chosen here as representative of all the other conditions in order to discuss the reduction process. Gaseous product distribution and feedstock conversions with respect to time are shown in Fig. 2. NiO reduction (R1) occurred initially, evidenced by H_2O formation which resulted in a negative H_2O conversion (Fig. 2b), and by a large amount of CO_2 production (Fig. 2a). NiO reduction with scrap tyre oil or bio-oil was also investigated in previous studies [31, 32], in which production plateaus of CO_2 and H_2O could be clearly identified. Unlike those almost exclusive reduction stages, an intermediate regime where reduction and reforming coexisted was shown in this study. The steam reforming reaction only lagged NiO reduction by around 10 seconds (Fig. 2c). Due to continuous generation of metallic Ni with catalytic activity, the production rate of CO and H_2 as indicators of reforming rate increased linearly. After about 360 seconds, the production rates of all gas products as well as feedstock conversions levelled off, suggesting NiO reduction had ended and steam reforming with water gas shift became dominant and stable. This was further supported by XRD data of the catalyst after reacting for 360 seconds (Fig. 3), which only exhibited the characteristic peaks of metallic Ni and α-Al_2O_3. Compared with the XRD pattern of the fresh catalyst, the disappearance of NiO diffraction peaks in the reacted catalyst indicated that NiO in the catalyst was completely reduced to metallic Ni.

However, when the reaction temperature fell to 500 °C, the reduction process could not proceed smoothly. Catalyst composition analysis based on XRD data showed that it took 1200 seconds to achieve the NiO to Ni conversion of 38.6%. For the other reaction temperatures (550 °C, 600 °C, 700 °C and 750 °C), 100% reduction could be obtained within hundreds of seconds depending on reaction temperature. Therefore, 550 °C is considered as the lowest auto-reduction temperature of this catalyst when using HAc aqueous solution (S/C=3).

Although the reduction had stopped, the calculated reduction rate did not return to zero (Fig. 4a) and consequently the calculated conversion was larger than 100% (Fig. 4b, kinetics model will be discussed later). This error was possibly caused by propagation of experimental error in the calculation from Eq.1 through to Eq.5 [26]. For this reason, kinetics modelling was performed only on the conversion range of 0-50%.

3.1.2 Kinetics modelling

Kinetics of many solid state reactions can be expressed by Eq. 6 or its integral form Eq. 7, where α is the conversion fraction of reactant in time t, k is the reaction rate constant, and f(α) or g(α) represent the reaction mechanism. The kinetic models generally used fall into three groups [33-35]: (1) diffusion models, (2) geometrical contraction models and (3) nucleation and nuclei growth models (Table 1).

$$\frac{d\alpha}{dt} = k \times f(\alpha) \qquad \text{(Eq. 6)}$$

$$g(\alpha) = \int \frac{d\alpha}{f(\alpha)} = k \times t \qquad \text{(Eq. 7)}$$

$$\alpha = 1 - \exp(-\beta \times t^m) \qquad \text{(Eq. 8)}$$

$$\ln\left(-\ln\left(1-\alpha\right)\right) = ln(\beta) + m \times ln(t) \qquad \text{(Eq. 9)}$$

Hancock and Sharp [34] have developed a convenient method for kinetic model-fitting of isothermal solid state reactions based on Avrami-Erofeyev equation (Eq. 8) and its transformation (Eq.9), where β is a constant, m depends on the geometry of reactant particles and reaction mechanism. It was pointed that experimental data obeying any one of the kinetic models in Table 1 gives rise to approximately linear plots of ln [− ln(1-α)] vs. ln t if the range of α is limited to 0.15-0.5. The gradient m of such plots could be used to help select the most suitable kinetic model. Theoretically, the m value is located around 0.5 for diffusion controlled reactions, around 1.0 for geometrical contraction controlled reactions, and 2.00 or 3.00 for nucleation and nuclei growth controlled reactions.

In the present study, the Hancock-Sharp method was employed. The m values for various temperatures or S/C ratios were between 1 and 2. It was difficult to distinguish among geometrical contraction models (R2, R3) and two-dimensional nucleation and nuclei growth model (A2) solely according to m values. Hence, g(α) against t based on R2, R3 and A2 models were plotted. Such plots should have been straight lines if the corresponding theoretical model was fitting. For this reason, the regression-squared value (R^2) of linear fit was used as a criterion of agreement with the theoretical models. The A2 and R3 models were found to have R^2 much closer to 1 compared with the R2 model, representing better fits. The change trends of m values and R^2 values with respect to temperature or S/C ratio are illustrated in Fig. 5. With temperature increasing from 550 to 650 °C or S/C ratio decreasing, m exhibited a rising trend. It suggested that a progressive mechanism change from R3 to A2 may have occurred. That was why the R^2 for the A2 model increased whereas the R^2

for the R3 model decreased, as shown in Fig. 5. After 650 °C, m was stable at about 1.75 and a satisfactory goodness of fit (with R^2 larger than 0.996) was attained for the A2 model. It indicated that the reduction reaction was isokinetic for the temperature range of 650-750 °C with S/C=3.

Normally, chemical reaction is the rate determining step of reactions which follow geometrical contraction models (or known as phase-boundary controlled models) [36, 37]. Geometrical contraction models assume that nucleation occurs rapidly on the surface of the solid reactant. A reaction interface moves from the edge of a cylinder (R2) or the surface of a sphere (R3) toward the solid reactant centre with a constant rate. Equations for geometrical contraction models are the same as those for a shrinking core model controlled by chemical reaction [18, 37, 38].

Nucleation and nuclei growth models (also known as Avrami-Erofeyev models) [33, 39, 40] give a typical S-shape for conversion α against t, starting slowly, rising rapidly, and then levelling off again. According to this model, the macroscopic conversion-time behaviour is determined by the relative rate of nucleation, nuclei growth and the concentration of potential germ nuclei. As for the dimensionality of nuclei growth, Kanervo et al.[41] pointed that three-dimensional nucleation and nuclei growth model (A3) is likely feasible only for reduction of bulk metal oxides while the A2 model is probably confined to reduction of supported oxide systems. In the present work, the A2 model is more acceptable than A3 because a Ni crystallite has a tendency to form a two-dimensional overlayer on the Al_2O_3 support.

Although many studies suggested that reduction kinetics of NiO, either bulk or supported, obeyed geometrical contraction models [18, 23, 37, 42, 43], nucleation and nuclei growth models also found applications in kinetic analysis of NiO reduction [38, 39, 44, 45]. Hossain et al. [39] compared the nucleation and nuclei growth model with the geometrical contraction model when studying reduction kinetics of a Co-Ni/Al_2O_3 catalyst. It was concluded that the adequacy of the nucleation model was superior to that of the geometrical contraction model for the studied system. Hardiman et al. [45] applied the nucleation and nuclei growth model (m=3) to fit their experimental data because the profile of conversion vs. time had a characteristic S-shape. In these two studies, however, the interpretation of kinetic model in terms of reaction mechanism was not clarified.

In the present study, the A2 model is considered as the best-fit kinetic model due to its higher R^2 values (>0.99) compared with the R3 model. The presence of water in reaction system could account for the fitness of A2 model. According to Richardson and Twigg [38], Ni atoms are liberated by NiO reduction and migrate across Al_2O_3 surface until they reach a nucleation site where nuclei are formed and grow into clusters and then crystallites. Water adsorbed on the catalyst surface retards nucleation by limiting the diffusion of Ni atoms across Al_2O_3 surface. It is also believed that the textural factors of the catalyst are very important in establishing the role of water [42]. The inhibition of water on nucleation is enhanced when hydrophilic additives, such as Ca and Mg, are present in the catalyst [17, 46]. In the current work, the nucleation rate of Ni atoms is extremely slow due to the considerable amount of water present. Therefore, nucleation and nuclei growth become the rate determining step.

3.1.3 Calculation of apparent activation energy (effects of temperature on rate constant)

The relation of reduction rate constant with temperature is represented by the Arrhenius equation (Eq. 10), where A is pre-exponential factor, E_a is the apparent activation energy and T is the absolute temperature. The rate constant k was obtained from the slope of A2(α) against t (A2(α)=[-ln(1-α)]$^{1/2}$). E_a was estimated from the slope of ln(k) versus 1/RT as shown in Fig. 6. The apparent activation energy of NiO reduction by HAc was therefore calculated to be 38 kJ per mol NiO for conversions below 50%, S/C=3 and in the temperature range of 550-750 °C. This is within the breadth of 14-114 kJ/mol when using H_2, CO or CH_4 as reducing agent [18, 23, 37, 39, 42, 43].

$$k = A exp(-\frac{E_a}{RT})$$
(Eq. 10)

3.1.4 Effects of water content on rate constant

As Fig. 7 shows, the rate constant of NiO reduction correlated to water content in the feed stream, which supported the argument that water has an important role in the reduction mechanism. The largest reduction rate constant was obtained when S/C=2. It is understandable that the reduction rate decreased as S/C ratio increased from 2 to 5 because water retained on catalyst surface may impede nucleation. To explain why the reduction rate constant for S/C=1 was smaller than that for S/C=2, a set of comparative experiments were carried out and their experimental conditions are listed in Table 2. After steam reforming experiments, TGA-FTIR tests were performed on the reacted catalyst under the same TPO condition. Their CO_2 chemigram profiles (amount of CO_2 emission vs. temperature) are displayed in Fig. 8.
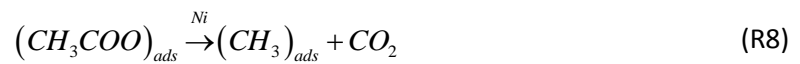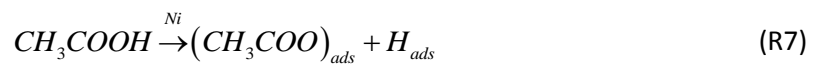
As shown in Fig. 8, there were two CO_2 emission peaks during the TPO of the run 1 sample. Normally, the combustion temperature of carbonaceous materials depends on their nature and deposition sites. It is reasonable to postulate that two different carbonaceous materials were deposited on the catalyst surface. They account for one CO_2 peak at 330°C and the other at 530 °C, respectively. For convenience, they are denoted as 330 CD ('carbon deposits') and 530 CD hereafter. The comparison of run 1 with run 2 (Fig. 8a) implies that 330 CD was formed during NiO reduction by HAc. The comparison of run 2 with run 3 (Fig. 8b) indicates that low water content caused the formation of 330 CD.

The existence of two CO_2 peaks during the TPO of used catalyst has been reported in literature [10, 47, 48]. It is generally assumed that the lower temperature peak (300 °C) is due to the coke deposited on active metal, while the higher temperature peak (550°C, the most significant one) is attributed to the coke formed on the support. In addition to different deposition sites, the structures of the two types of coke are also different. The former consists of polyaromatic compounds whereas the latter has a pseudo-graphitic structure.

In the present work, the CO_2 profile from bare Al_2O_3 sample (Fig. 8c) confirms that 530 CD was formed, at least partially, due to reactions occurring on Al_2O_3. Ketonization of HAc (R6) to produce acetone is a common reaction when support materials are used without active phase [1, 10]. Acetone produced could further undergo oligomerization reactions via intermediates such as mesityl oxide and ketene, resulting in coke formation [14]. This type of coke may contribute to the CO_2 peak of 530 °C. The reactions causing the 330 CD will be discussed below.

$$2CH_3COOH \rightarrow CH_3COCH_3 + CO_2 + H_2O \tag{R6}$$
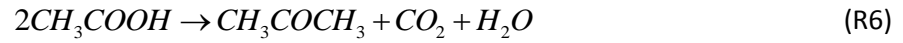
As has been described in literature [21, 42, 49], the first step of reduction is the dissociation of the reducing agent to form adsorbed radical species, initially by NiO, then by metallic Ni as it becomes available. In the case of using HAc as reductant, a series of dissociation reactions (R7-9) are understood to take place, resulting in the production of adsorbed radicals H_{ads} and $(CH_{1-3})_{ads}$ [8]. Desorption and re-adsorption of these radicals may take place on catalyst surface [21, 50]. The H_{ads} radical formed on Ni sites either plays the role of reducing species when re-adsorbed onto NiO surface or produces H_2 when combining with each other. $(CH_{1-3})_{ads}$ may also desorb from Ni surface, diffuse and then adsorb on the NiO surface where NiO reduction occurs. The desorption of radicals from Ni and re-adsorption onto NiO are essential for the reduction of NiO [21]. For those $(CH_{1-3})_{ads}$ still adsorbed on Ni surface, there are two possible reaction pathways. One is to be gasified by steam to produce CO and H_2 (steam reforming, R10). The other is to be further oligomerized and deposited on Ni sites (coke formation, R11). In the present work, $(CH_{1-3})_{ads}$ on Ni sites could not be gasified sufficiently due to the low steam content (S/C=1), and hence formed coke which contributed to the CO_2 peak at 330 °C. Coke deposited on Ni impaired the dissociation of HAc and the formation of reducing species, leading to a low reduction rate. This is why the reduction rate constant was less for S/C=1 than that for S/C=2. The presence of water in feedstock does not always have a negative effect on NiO reduction. The optimal S/C ratio for NiO reduction with HAc was found here to be 2. According to the discussion above, the reduction reaction mechanism is illustrated in Fig. 9.

$$CH_3COOH \xrightarrow{Ni} (CH_3COO)_{ads} + H_{ads} \tag{R7}$$

$$(CH_3COO)_{ads} \xrightarrow{Ni} (CH_3)_{ads} + CO_2 \tag{R8}$$

$$(CH_3)_{ads} \xrightarrow{Ni} C_{ads} + 3H_{ads} \tag{R9}$$

$$C_{ads} + H_2O \xrightarrow{Ni} CO + H_2 \tag{R10}$$

$$nC_{ads} \rightarrow coke \tag{R11}$$

3.2 Steam reforming performance in the integrated process

The integrated catalyst reduction and steam reforming process has been examined at a series of temperatures or with different S/C ratios. Only H_2, CO_2, CO and small quantities of CH_4 were detected in the reformate. Average values of feedstock conversions, H_2 yield and gas concentrations over the test period are used to demonstrate the effects of temperature or S/C ratio on steam reforming performance in such an integrated process. Previous studies [1, 10] have shown that there is a complex reaction network during steam reforming of HAc on Ni based catalysts. Apart from the steam reforming reaction (R2) and water gas shift (R3), several side reactions like thermal decomposition ($CH_3COOH \rightarrow CH_4 + CO_2$), ketonization (R6), and CO disproportionation 'Boudouard reaction' ($2CO \square \ CO_2 + C$) may take place as well.

3.2.1 Effects of temperature

Fig. 10 shows the influence of reaction temperature on steam reforming performance of HAc. As Fig. 10a reveals, the H_2 yield increased along with the HAc conversion although the H_2O conversion almost remained unchanged with increasing temperature. The rise in HAc conversion is attributed to the facilitation of the steam reforming reaction (endothermic) by elevated temperatures. The constant H_2O conversion was a combined effect of promoted steam reforming reaction and restrained water gas shift (exothermic) at high temperatures. As for the composition of the reformate (Fig. 10b), the H_2 concentration seemed unaffected by temperature in the range studied, but concentrations of the other three gases changed with temperature. CH_4 concentration dropped to approximately zero as temperature increased possibly due to the enhancement of CH_4 steam reforming (endothermic). The contribution of CH_4 steam reforming to H_2 concentration compensated the decrease of H_2 concentration due to the inhibition of water gas shift by high temperature, which made the H_2 concentration level off. Meanwhile, the inhibition of both water gas shift and Boudouard reactions (exothermic), led to an increase in CO concentration and a decrease in CO_2 concentration.

With a reaction temperature below 650 °C, there was a large amount of carbon deposits on the reactor wall produced from the Boudouard reaction. When the temperature was raised to 650 °C or above, the carbon formation on reactor wall could be eliminated. Therefore, 650 °C is suggested as the lowest temperature for steam reforming of HAc in such an integrated process.

3.2.2 Effects of S/C ratio

The effect of S/C ratio on the steam reforming performance of HAc is exhibited in Fig. 11. As shown in Fig. 11a, the HAc conversion and the H_2 yield increased with rising S/C ratio. This was expected due to the fact that increased water content promotes a favourable shift in the reaction equilibrium of both steam reforming and water gas shift. The promoted water gas shift reaction also resulted in CO concentration decreasing and CO_2 concentration increasing as illustrated in Fig. 11b. The decrease in H_2O conversion could be ascribed to increased feed of water. Apart from steam reforming and water gas shift reactions, the CH_4 steam reforming reaction was also favoured at high S/C ratio, leading to a decreasing tendency for CH_4 concentration. At S/C=3, the amount of CH_4 in the

reformate was negligible. As expected, both enhancement of CH_4 steam reforming and water gas shift contributed to an increase in H_2 concentration and yield.

The steam reforming activity of HAc obtained in this integrated process is comparable with results obtained via a conventional steam reforming process by other groups [11-13, 51, 52] (summarised in Table 3).

3.2.3 Comparison of experimental data with thermodynamic equilibrium data

The results of thermodynamic equilibrium calculation for HAc steam reforming are also illustrated in Fig. 10 and Fig. 11 (in dash line). The HAc conversion reaches 100% at equilibrium for the conditions studied herein, which are not plotted in figures. According to Le Chatelier's principle, the endothermic steam reforming reaction (R2, ΔH_{298K}=170.8 kJ/mol HAc) is favoured by increasing both temperature and steam content. Conversely, the exothermic water gas shift (R3, ΔH_{298K} =-41.2 kJ/mol CO) is adversely affected by increasing temperature, but favoured by increasing steam content. The adverse effect of temperatures on water gas shift results in a small decrease in water conversion and H_2 yield at equilibrium from 550 to 750 °C with S/C=3 (Fig. 10). Compared to the equilibrium data, a lower H_2 yield (around 25% lower than its counterpart at equilibrium at 750 °C) was shown in the experiment, along with lower conversions of HAc and water. The main reason for the discrepancy between the equilibrium data and the experimental data is the kinetic limitation of the steam reforming reaction. Some of HAc molecules and intermediate products do not have enough time to react with water over the catalyst before being flushed out of the reactor. With temperature increasing, this gap decreases suggesting that the steam reforming reaction is accelerated at high temperature and gets closer to equilibrium. Compared to temperature, the effects of S/C ratio on H_2 yield and water conversion at equilibrium are more evident (Fig. 11). Moreover, their change trends are nearly consistent with those obtained in experiment, resulting in a stable discrepancy of approximately 30% for H_2 yield. Although the feedstock conversion and H_2 yield are far from equilibrium due to the kinetic limitation, the gaseous product composition shows a good agreement with the equilibrium values except for a slightly higher CO_2 concentration and lower H_2 concentration. In summary, the improvement of kinetics by elevating temperature, increasing the contact time of HAc with catalyst (decrease the weight hourly space velocity), or using catalysts with high activity will bring the steam reforming performance closer to its thermodynamic equilibrium.

3.2.4 HAc auto-reduced and H_2-reduced catalyst activities in steam reforming

Compared with a conventional steam reforming, a basic distinction of an integrated process is that NiO is auto-reduced by the reforming feedstock. It is well known that reduction process greatly affects catalyst activity in steam reforming because reduction parameters may determine metal dispersion, crystallite size, etc. To find out the difference between the catalyst auto-reduced by HAc and the H_2-reduced catalyst, two groups of comparative experiments were conducted. For convenience, samples are denoted as 'HAc sample' and 'H_2 sample', respectively. The reacted catalyst samples were characterised by XRD and CHN elemental analysis to obtain Ni crystallite size and carbon content (wt% on the basis of Ni/Al_2O_3). TOC and ICP tests were used to detect carbon

content and Ni ion content in the condensate samples collected. Experimental conditions and test results are listed in Table 4. As shown, steam reforming activity slightly declined when the catalyst was reduced by HAc compared with by H_2.

Analysis of XRD data showed that the Ni crystallite sizes of both HAc and H_2 samples were located in the 33-34 nm range. The influence on Ni crystallite size of using HAc to reduce the NiO/Al_2O_3 catalyst was not evident.

With respect to carbon element distribution, there was a remarkable difference between the integrated process and the conventional process. The HAc sample showed less carbon deposits on the used catalyst and a slightly lower carbon conversion to gases, but exhibited larger carbon content in the liquid condensate than the H_2 sample. This suggested more intermediate products such as acetone were formed in the auto-reducing integrated process.

ICP results revealed that some Ni element broke away from the catalyst and flowed into the condensate during reactions. HAc reacts with neither NiO nor Ni at room temperature. However, in the steam reforming process, the high temperature as well as the presence of steam makes the corrosion of NiO or Ni by HAc possible. Compared to the H_2 sample, Ni loss from the HAc sample was more considerable. This could account for the small drop in steam reforming activity [6].

Fig. 12 shows SEM images of the reacted catalyst samples. It was found that carbon deposits were not evenly distributed on the catalyst surface in the integrated process. Some parts of the catalyst surface were almost free of carbon deposits (Fig. 12a) whereas others were covered by dense carbon filaments (Fig. 12 b and c). It was also noted that the carbon deposits of HAc sample was comprised of large carbon filaments (300 nm in diameter) and small carbon filaments (10 nm in diameter) (Fig. 12b). In contrast, the H_2 sample only had medium sized filaments (50 nm in diameter) as shown in Fig. 12d. The comparison of Fig. 12c and Fig. 12d revealed that carbon deposits on the HAc sample were denser than those on the H_2 sample. Denser carbon deposits mean more resistance for steam and fuel molecules to reach active sites. This may be another reason for the slight decrease in steam reforming activity in the integrated process.

4. Conclusions

An integrated process featuring auto-reduction of catalyst by reforming feedstock acetic acid (HAc) and subsequent steam reforming was proposed in this paper. This process was investigated at different temperatures with different molar steam to carbon ratios (S/C) over a NiO/Al_2O_3 catalyst. At 650 °C and S/C=3, the steam reforming reaction took place instantly following NiO reduction with a lag time of only 10 seconds, and 100% reduction could be achieved in 360 seconds. The best fitting kinetic model for NiO reduction (0-50% conversion) was the two-dimensional nucleation and nuclei growth model (A2). Its corresponding apparent activation energy was 38 kJ/mol over 550-750 °C. In addition to temperature, steam content in the feed also affected reduction kinetics. S/C=2 was found to be optimal for NiO reduction. When low steam content (e.g. S/C=1) was applied, CH_{1-3} radicals adsorbed on Ni sites could not be gasified sufficiently by steam. As a result, carbon

deposited on Ni impaired HAc dissociation and hence lowered the reduction rate. Accordingly, a mechanism of NiO auto-reduction by HAc was proposed.

With respect to catalyst activity, a slight decrease was shown in the integrated process, compared to a conventional steam reforming process. This is likely attributed to more Ni element lost to the condensate when using HAc to reduce the catalyst. Another possible reason is that the catalyst surface was covered by denser carbon filaments, which impeded the access of reactant molecules to active sites. Despite of the small activity degradation, a H_2 purity of 58.68%, a H_2 yield of 63.17% (i.e 76.4% of the equilibrium value) and HAc conversion of 88.97% were achieved under reaction conditions of 750 °C and S/C=3.

In such an integrated process, the effect of temperature on the reduction rate was consistent with that on steam reforming activity. 650 °C was found to be the lowest temperature to afford fast reduction kinetics without CO disproportionation. However, the S/C ratio had an opposite effect on the reduction rate and the steam reforming activity. A rise in S/C ratio increased steam reforming activity as expected, but led to a decrease in the reduction rate. Hence, a changing S/C regime may need to be applied in an integrated process. Furthermore, the cyclic behaviour of catalyst in alternating fuel feed and air feed will be investigated for the potential application of bio-feedstock in chemical looping reforming.

Acknowledgments

Reference

[1] Trane R, Dahl S, Skjoth-Rasmussen MS, Jensen AD. Catalytic steam reforming of bio-oil. International Journal of Hydrogen Energy 2012;37:6447-72.

[2] Wang D, Czernik S, Montane D, Mann M, Chornet E. Biomass to hydrogen via fast pyrolysis and catalytic steam reforming of the pyrolysis oil or its fractions. Industrial & Engineering Chemistry Research 1997;36:1507-18.

[3] Garcia-Perez M, Chaala A, Pakdel H, Kretschmer D, Roy C. Characterization of bio-oils in chemical families. Biomass & Bioenergy 2007;31:222-42.

[4] Hu X, Lu GX. Investigation of the steam reforming of a series of model compounds derived from bio-oil for hydrogen production. Applied Catalysis B: Environmental 2009;88:376-85.

[5] Ramos MC, Navascues AI, Garcia L, Bilbao R. Hydrogen production by catalytic steam reforming of acetol, a model compound of bio-oil. Industrial & Engineering Chemistry Research 2007;46:2399-406.

[6] Wu C, Liu RH. Sustainable hydrogen production from steam reforming of bio-oil model compound based on carbon deposition/elimination. International Journal of Hydrogen Energy 2011;36:2860-8.

[7] Comas J, Marino F, Laborde M, Amadeo N. Bio-ethanol steam reforming on Ni/Al$_2$O$_3$ catalyst. Chemical Engineering Journal 2004;98:61-8.

[8] Wang D, Montane D, Chornet E. Catalytic steam reforming of biomass-derived oxygenates: Acetic acid and hydroxyacetaldehyde. Applied Catalysis A: General 1996;143:245-70.

[9] Zheng XX, Yan CF, Hu RR, Li J, Hai H, Luo WM, et al. Hydrogen from acetic acid as the model compound of biomass fast-pyralysis oil over Ni catalyst supported on ceria-zirconia. International Journal of Hydrogen Energy 2012;37:12987-93.

[10] Basagiannis AC, Verykios XE. Reforming reactions of acetic acid on nickel catalysts over a wide temperature range. Applied Catalysis A: General 2006;308:182-93.

[11] Hu X, Lu G. Comparative study of alumina-supported transition metal catalysts for hydrogen generation by steam reforming of acetic acid. Applied Catalysis B: Environmental 2010;99:289-97.

[12] Basagiannis AC, Verykios XE. Catalytic steam reforming of acetic acid for hydrogen production. International Journal of Hydrogen Energy 2007;32:3343-55.

[13] Thaicharoensutcharittham S, Meeyoo V, Kitiyanan B, Rangsunvigit P, Rirksomboon T. Hydrogen production by steam reforming of acetic acid over Ni-based catalysts. Catalysis Today 2011;164:257-61.

[14] Takanabe K, Aika K, Seshan K, Lefferts L. Catalyst deactivation during steam reforming of acetic acid over Pt/ZrO$_2$. Chemical Engineering Journal 2006;120:133-7.

[15] Goodman DR. Handling and using catalysts in the plant. In: Twigg MV, editor. Catalyst handbook. 2nd ed. London: Manson Publishing Ltd; 1996, p. 161-188.

[16] Ryden M, Lyngfelt A, Mattisson T. Chemical-looping combustion and chemical-looping reforming in a circulating fluidized-bed reactor using Ni-based oxygen carriers. Energy & Fuels 2008;22:2585-97.

[17] Richardson JT, Scates RM, Twigg MV. X-ray diffraction study of the hydrogen reduction of NiO/α-Al$_2$O$_3$ steam reforming catalysts. Applied Catalysis A: General 2004;267:35-46.

[18] Utigard TA, Wu M, Plascencia G, Marin T. Reduction kinetics of Goro nickel oxide using hydrogen. Chemical Engineering Science 2005;60:2061-8.

[19] Ishida M, Jin HG, Okamoto T. A fundamental study of a new kind of medium material for chemical-looping combustion. Energy & Fuels 1996;10:958-63.

[20] Alizadeh R, Jamshidi E, Ale-Ebrahim H. Kinetic study of nickel oxide reduction by methane. Chemical Engineering & Technology 2007;30:1123-8.

[21] Syed-Hassan SSA, Li CZ. NiO reduction with hydrogen and light hydrocarbons: Contrast between SiO2-supported and unsupported NiO nanoparticles. Applied Catalysis A: General 2011;398:187-94.

[22] Zafar Q, Mattisson T, Gevert B. Integrated hydrogen and power production with CO$_2$ capture using chemical-looping reforming-redox reactivity of particles of CuO, Mn$_2$O$_3$, NiO, and Fe$_2$O$_3$ using SiO$_2$ as a support. Industrial & Engineering Chemistry Research 2005;44:3485-96.

[23] Abad A, Garcia-Labiano F, de Diego LF, Gayan P, Adanez J. Reduction kinetics of Cu-, Ni-, and Fe-based oxygen carriers using syngas (CO + H$_2$) for chemical-looping combustion. Energy & Fuels 2007;21:1843-53.

[24] Dupont V, Ross AB, Hanley I, Twigg MV. Unmixed steam reforming of methane and sunflower oil: A single-reactor process for -rich gas. International Journal of Hydrogen Energy 2007;32:67-79.

[25] Cho P, Mattisson T, Lyngfelt A. Comparison of iron-, nickel-, copper- and manganese-based oxygen carriers for chemical-looping combustion. Fuel 2004;83:1215-25.

[26] Pimenidou P, Rickett G, Dupont V, Twigg MV. High purity H_2 by sorption-enhanced chemical looping reforming of waste cooking oil in a packed bed reactor. Bioresource Technology 2010;101:9279-86.

[27] McCusker LB, Von Dreele RB, Cox DE, Louer D, Scardi P. Rietveld refinement guidelines. Journal of Applied Crystallography 1999;32:36-50.

[28] Kee RJ, Rupley FM, Miller JA. Chemkin-II: A fortran chemical kinetics package for the analysis of gas-phase chemical kinetics. Sandia National Laboratories; 1992 April. Report No.: SAND89-8009B.

[29] Chao J, Hall KR, Marsh KN, Wilhoit RC. Thermodynamic properties of key organic oxygen compounds in the carbon range C_1 to C_4 2. Ideal-gas properties. Journal of Physical and Chemical Reference Data 1986;15:1369-436.

[30] McBride BJ, Gordon S, Reno MA. Coefficients for calculating thermodynamic and transport properties of individual species. 1993 October. Report No.: NASA report TM-4513.

[31] Giannakeas N, Lea-Langton A, Dupont V, Twigg MV. Hydrogen from scrap tyre oil via steam reforming in a packed bed reactor. Applied Catalysis B: Environmental 2012;126:249-57.

[32] Lea-Langton A, Zin RM, Dupont V, Twigg MV. Biomass pyrolysis oils for hydrogen production using chemical looping reforming. International Journal of Hydrogen Energy 2012;37:2037-43.

[33] Khawam A, Flanagan DR. Solid-state kinetic models: Basics and mathematical fundamentals. Journal of Physical Chemistry B 2006;110:17315-28.

[34] Hancock JD, Sharp JH. Method of comparing solid-state kinetic data and its application to decomposition of kaolinite, brucite, and $BaCo_3$. Journal of the American Ceramic Society 1972;55:74-77.

[35] Go KS, Son SR, Kim SD. Reaction kinetics of reduction and oxidation of metal oxides for hydrogen production. International Journal of Hydrogen Energy 2008;33:5986-95.

[36] Gardner RA. Kinetics of silica reduction in hydrogen. Journal of Solid State Chemistry 1974;9:336-44.

[37] Szekely J, Lin CI, Sohn HY. Structural model for gas-solid reactions with a moving boundary 5. Experimental study of reduction of porous nickel-oxide pellets with hydrogen. Chemical Engineering Science 1973;28:1975-89.

[38] Richardson JT, Lei M, Forster K, Twigg MV. Reduction of model steam reforming catalysts NiO/α-Al_2O_3. Applied Catalysis A: General 1994;110:217-37.

[39] Hossain MM, de Lasa HI. Reactivity and stability of Co-Ni/Al_2O_3 oxygen carrier in multicycle CLC. Aiche Journal 2007;53:1817-29.

[40] Kanervo JM, Krause AOI. Kinetic analysis of temperature-programmed reduction: Behavior of a CrO_x/Al_2O_3 catalyst. The Journal of Physical Chemistry B 2001;105:9778-84.

[41] Kanervo JM, Krause AOI. Characterisation of supported chromium oxide catalysts by kinetic analysis of H2-TPR data. Journal of Catalysis 2002;207:57-65.

[42] Richardson JT, Scates R, Twigg MV. X-ray diffraction study of nickel oxide reduction by hydrogen. Applied Catalysis A: General 2003;246:137-50.

[43] Zafar Q, Abad A, Mattisson T, Gevert B. Reaction kinetics of freeze-granulated NiO/MgAl$_2$O$_4$ oxygen carrier particles for chemical-looping combustion. Energy & Fuels 2007;21:610-8.

[44] Hossain MM, de Lasa HI. Chemical-looping combustion (CLC) for inherent separations—a review. Chemical Engineering Science 2008;63:4433-51.

[45] Hardiman KA, Hsu CH, Ying TT, Adesina AA. The influence of impregnating pH on the postnatal and steam reforming characteristics of a Co-Ni/Al$_2$O$_3$ catalyst. Journal of Molecular Catalysis A: Chemical 2005;239:41-8.

[46] Richardson JT, Turk B, Twigg MV. Reduction of model steam reforming catalysts: Effect of oxide additives. Applied Catalysis A: General 1996;148:97-112.

[47] Barbier J. Deactivation of reforming catalysts by coking - a review. Applied Catalysis 1986;23:225-43.

[48] Duprez D, Demicheli MC, Marecot P, Barbier J, Ferretti OA, Ponzi EN. Deactivation of steam-reforming model catalysts by coke formation 1. Kinetics of the formation of filamentous carbon in the hydrogenolysis of cyclopentane on Ni/Al$_2$O$_3$ catalysts. Journal of Catalysis 1990;124:324-35.

[49] Ostrovski O, Zhang GQ. Reduction and carburization of metal oxides by methane-containing gas. Aiche Journal 2006;52:300-10.

[50] Lee WJ, Li C-Z. Coke formation and reaction pathways of catalyst-surface-generated radicals during the pyrolysis of ethane using Ni mesh catalyst. Applied Catalysis A: General. 2007;316:90-9.

[51] An L, Dong CQ, Yang YP, Zhang JJ, He L. The influence of Ni loading on coke formation in steam reforming of acetic acid. Renewable Energy 2011;36:930-5.

[52] Hu X, Lu GX. Inhibition of methane formation in steam reforming reactions through modification of Ni catalyst and the reactants. Green Chemistry 2009;11:724-32.

Table 1 Kinetic models of solid state reactions [33-35]

Model	$g(\alpha)$	m
One-dimensional diffusion (D1)	α^2	0.62
Two-dimensional diffusion (D2)	$(1-\alpha)\ln(1-\alpha)$	0.57
Three-dimensional diffusion by Jander (D3)	$[1-(1-\alpha)^{1/3}]^2$	0.54
Three-dimensional diffusion by Ginstling-Brounshtein (D4)	$1-2\alpha/3-(1-\alpha)^{2/3}$	0.57
geometrical contraction (cylinder) (R2)	$1-(1-\alpha)^{1/2}$	1.11
geometrical contraction (sphere) (R3)	$1-(1-\alpha)^{1/3}$	1.07
Two-dimensional nucleation and nuclei growth (A2)	$[-\ln(1-\alpha)]^{1/2}$	2.00
Three-dimensional nucleation and nuclei growth (A3)	$[-\ln(1-\alpha)]^{2/3}$	3.00

Table 2 Reaction conditions for a set of comparative experiments

Run no.	Solid material	Reduced by	S/C
1	NiO/Al_2O_3	HAc	1
2	NiO/Al_2O_3	H_2	1
3	NiO/Al_2O_3	HAc	2
4	bare Al_2O_3	---	1

Table 3 Steam reforming of HAc for H_2 production in literature

catalyst	Temperature (°C)	S/C	HAc conversion (%)	H_2 yield(%)	Reference
15%Ni/Al_2O_3	600	2	45	28	[51]
17%Ni/Al_2O_3	750	1.5	80	79.2	[12]
20%%Ni/Al_2O_3	400	2.5	80	52	[11]
30%Ni/Al_2O_3	400	7.5	67.8	66.2	[52]
15%Ni/Al_2O_3	650	3	75	66	[13]
		6	95	92	
18% NiO/Al_2O_3	750	3	88.97	63.17	present work
	650	3	74.51	53.16	

Table 4 Comparison of the integrated process and conventional steam reforming process

Run no.	Conditions		Reforming activity		Characterization results			
	Reductant	S/C	HAc conversion (%)	H_2 yield (%)	C_s content (wt%)	C_l content (g/L)	Ni content (mg/L)	Ni crystallite size (nm)
5	HAc	2	67.41	46.09	1.90	88.20	89.73	33.57
6	H_2	2	73.25	50.19	2.19	77.17	64.50	33.15
7	HAc	1	65.21	39.00	2.64	133.13	333.45	33.83
8	H_2	1	71.49	43.68	3.14	128.22	247.30	34.08

Note: all experiments were performed at 650 °C with the same HAc flow rate

C_s: carbon on catalyst

C_l: carbon in condensate

Figure captions

Fig. 1 Schematic diagram of experimental set-up

Fig. 2 An integrated catalyst reduction and steam reforming experiment at 650 °C with S/C=3 (a) the rate of gas production; (b) feedstock conversion and (c) zoom in the onset of reactions

Fig. 3 XRD patterns of (a) the catalyst reacting for 360 s and (b) fresh catalyst:
(o) Ni characteristic peaks, (+) NiO characteristic peaks, the other unmarked peaks are attributed to α-Al_2O_3

Fig. 4 NiO reduction by HAc during an integrated process at 650 °C with S/C=3 (a) curve of reduction rate vs. time and (b) conversion fraction from NiO to Ni vs. time

Fig. 5 Change trend of m values and R^2 values of kinetic models (A2 or R3) with (a) temperatures or (b) S/C ratios
A2: two-dimensional nucleation model
R3: geometrical contraction model of sphere
R^2: regression-squared value of linear fitting

Fig .6 Arrhenius plot of NiO reduction by HAc solution with S/C=3 for the NiO to Ni conversion range of 0-50%

Fig. 7 Influence of water content on reduction rate constant and reduction time at 650 °C

Fig. 8 CO_2 chemigram profiles of a set of comparative experiments (a) different reducing agents (b) different S/C ratios (c) NiO/Al_2O_3 catalyst and bare Al_2O_3

Fig. 9 Mechanism diagram of NiO/Al_2O_3 catalyst reduction by HAc

Fig. 10 Effects of temperature on steam reforming performance at S/C=3 (a) feedstock conversion and H_2 yield (b) gaseous product distribution (solid line: experimental data, dash line: thermodynamic equilibrium data)

Fig. 11 Effects of S/C ratio on steam reforming performance at 650 °C (a) feedstock conversion and H_2 yield (b) gaseous product distribution (solid lines: experimental data, dash lines: thermodynamic equilibrium data)

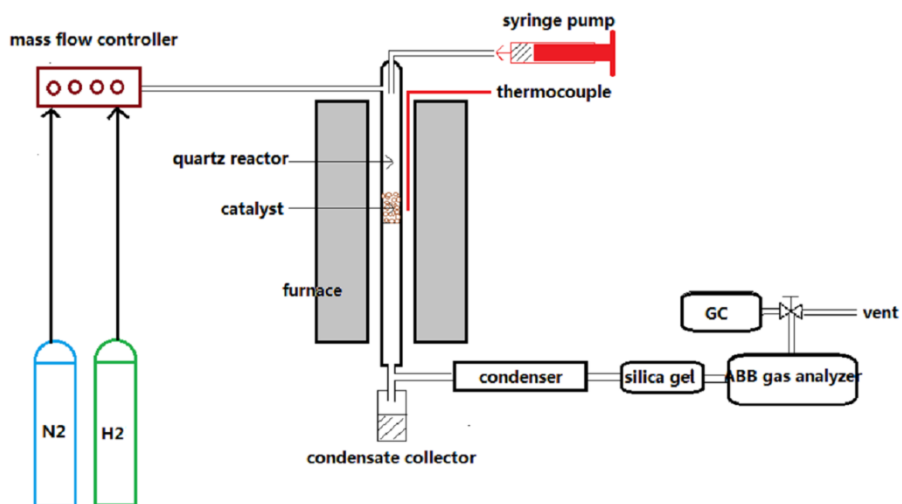Fig. 12 SEM images of reacted catalyst (a-c) different sites of catalyst reduced by HAc (d) catalyst reduced by H_2
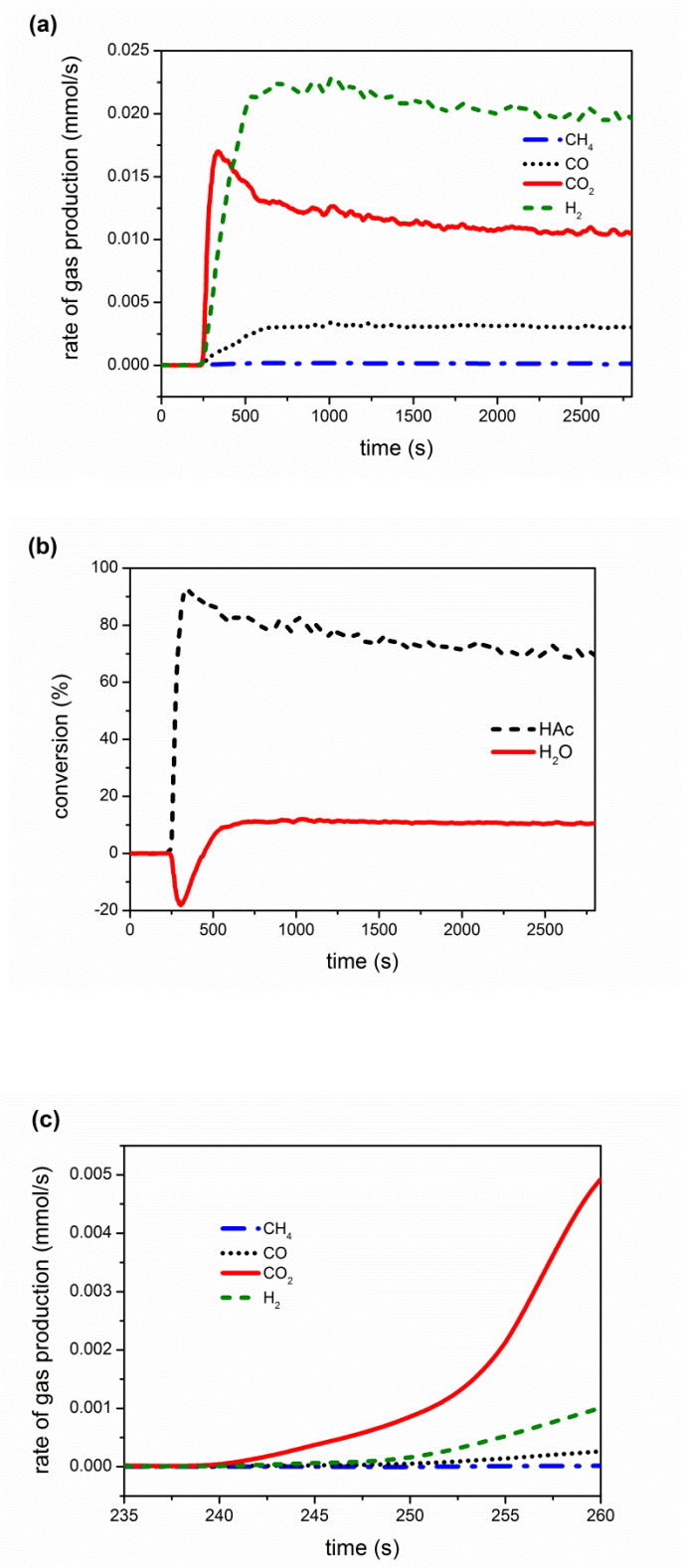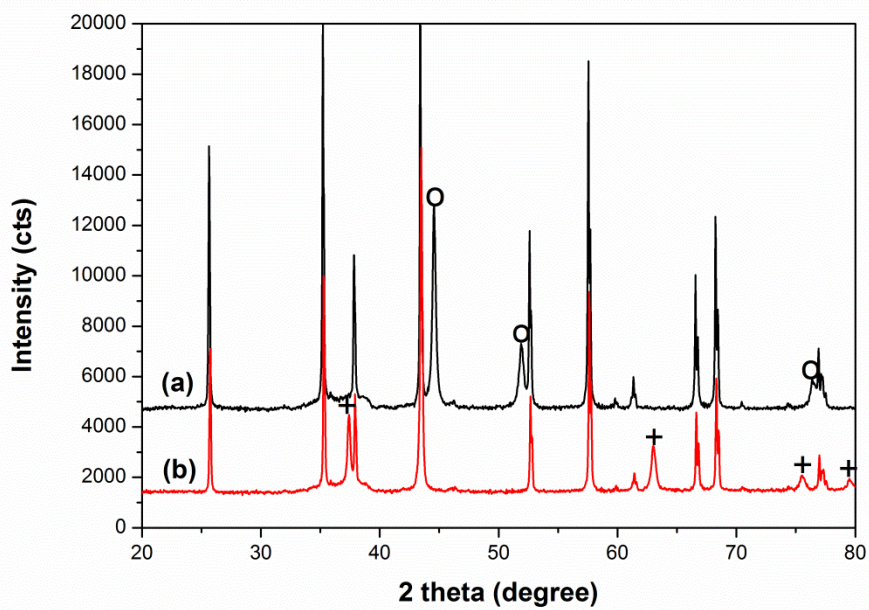
Fig. 1

Fig. 2

(a)

(b)

(c)

Fig. 3

Fig. 4
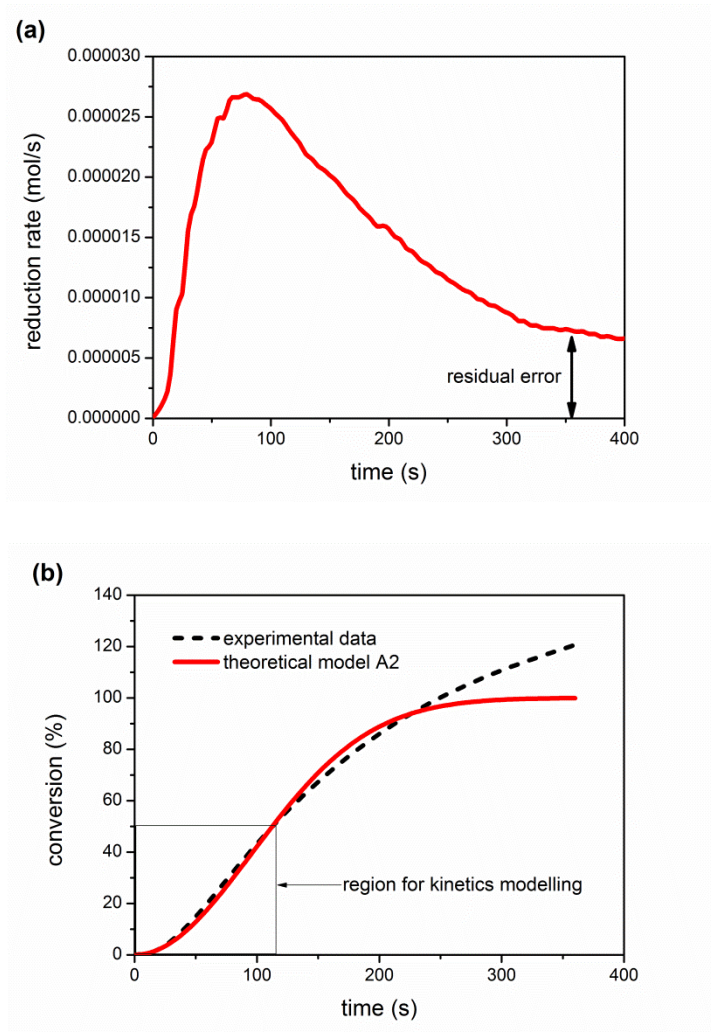
Fig. 5
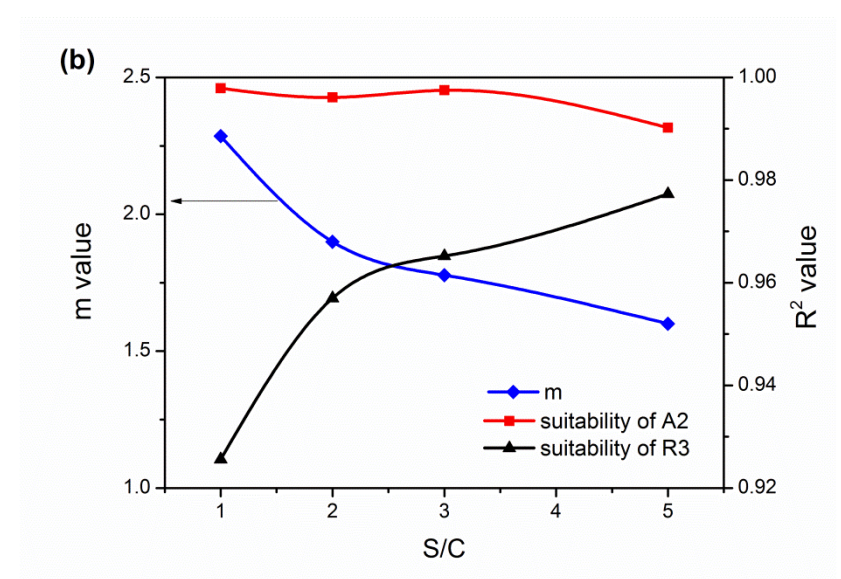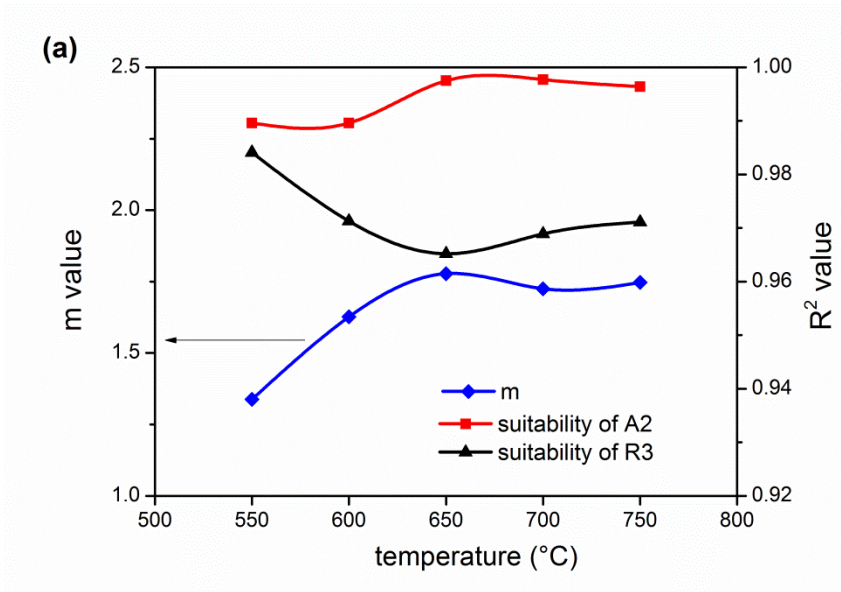
Fig. 6
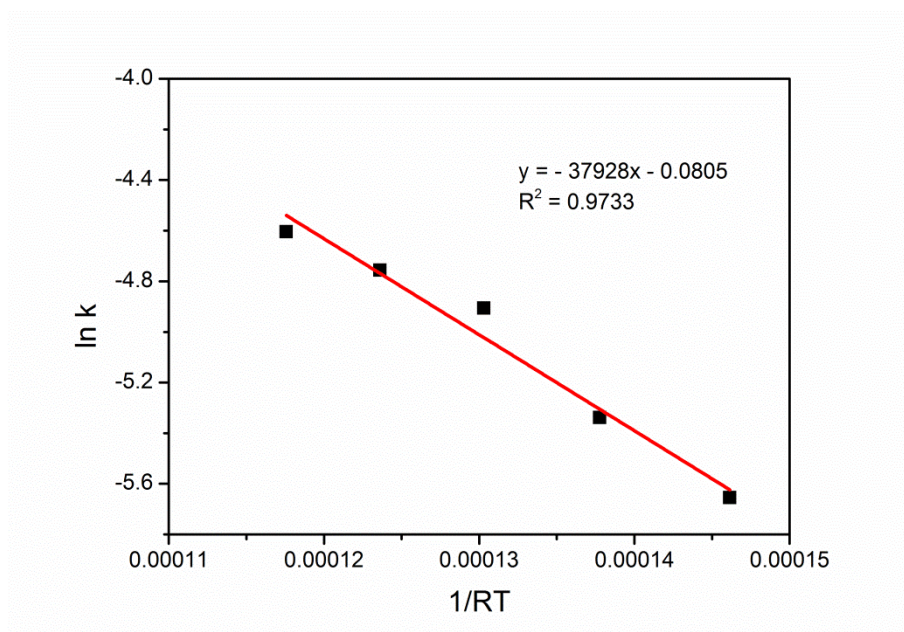
Fig. 7
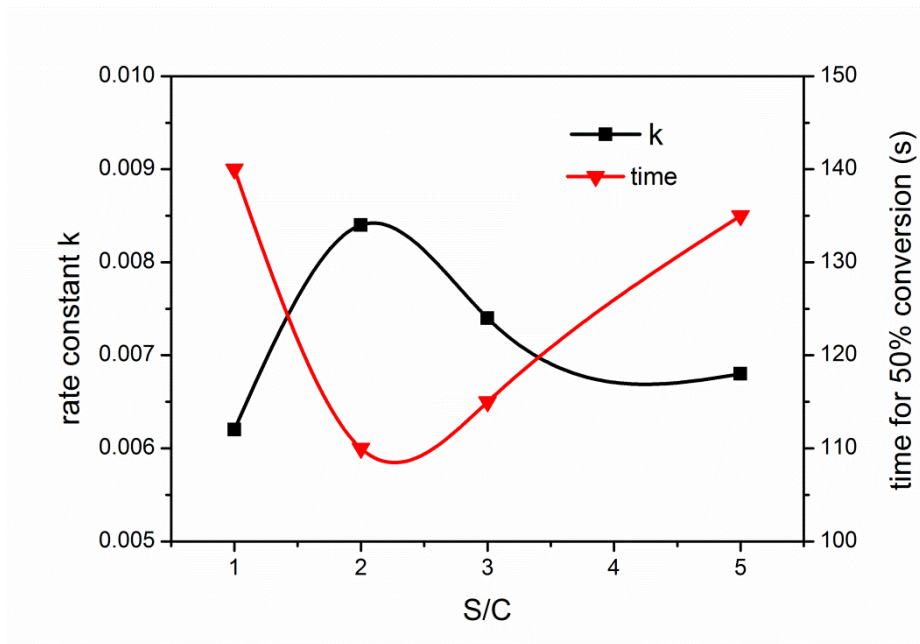
Fig. 8

Fig. 9

Fig. 10

Fig. 11

Fig. 12

(a)

200 nm | Mag = 70.00 K X | Signal A = InLens | LEMAS
| EHT = 3.00 kV | WD = 3.6 mm | Date :28 Mar 2013

(b)

200 nm | Mag = 70.00 K X | Signal A = InLens | LEMAS
| EHT = 10.00 kV | WD = 7.9 mm | Date :13 Mar 2013

(c)

200 nm | Mag = 70.00 K X | Signal A = InLens | LEMAS
| EHT = 3.00 kV | WD = 4.6 mm | Date :28 Mar 2013

(d)

200 nm | Mag = 70.57 K X | Signal A = InLens | LEMAS
| EHT = 3.00 kV | WD = 3.8 mm | Date :14 Feb 2013